Artificial Intelligence in the NASA Volcano Sensorweb: Over a Decade in Operations

Ashley G. Davies, Steve Chien, Joshua Doubleday, Daniel Tran, David Mclaren

Jet Propulsion Laboratory, California Institute of Technology, USA
e-mail: firstname.lastname@jpl.nasa.gov

Abstract

Volcanic activity can occur with little or no warning. Increasing numbers of space borne assets can enable coordinated measurements of volcanic events to enhance both scientific study and hazard response. We describe the use of space and ground measurements to target further measurements as part of a worldwide volcano monitoring system. We utilize a number of alert systems including the MODVOLC, GOESVOLC, US Air Force Weather Advisory, and Volcanic Ash Advisory Center (VAAC) alert systems. Additionally we use in-situ data from ground instrumentation at a number of volcanic sites, including Iceland.

Artificial Intelligence Software plays a key role in the Volcano Sensorweb. First, several in-situ volcano monitoring networks use "intelligent" data interpretation software to trigger alerts that can then be used to allocate network resources, notify human agents, and even task space observations. Second, the Earth Observing One (EO-1) spacecraft uses Artificial Intelligence Software to automatically task the spacecraft to execute observations. Third, EO-1 also interprets thermal data onboard to allow for faster notifications of volcanic activity. Finally some data interpretation steps use intelligent software such as Random Decision Forest Methods used to automatically estimate volcanic plume heights in Worldview-2 Imagery.

1 Introduction

The study of volcanoes is important for both scientific and humanitarian reasons. From a scientific standpoint, volcanic gas and ash emissions contribute significantly to the terrestrial atmosphere. Ash depositions and lava flows can also greatly affect local environments. From a humanitarian standpoint many people live within a short distance of active volcanoes and therefore can be affected via both atmospheric (ash, debris) and lava flow phenomena.

Satellite study of volcanoes is very useful because it can provide data for large areas of the Earth's surface with a range of modalities ranging form visible to infra-red, radar and beyond. Satellite sensing can also access remote locations and hazardous regions without difficulty. One issue with space-based volcano measurement is that atmospheric conditions (e.g. clouds) can interfere with many sensors (visible, IR). Additionally, for taskable (e.g., point and shoot) sensors, satellite contention for targets is high (e.g. other targets may be competing for observation time) so that knowledge of specific volcanic activity (e.g. timely alerts) may be required in order to task to acquire volcanic imagery.

In-situ sensing can provide a valuable range of complementary information such as seismographic, discharge, acoustic, and other data. However many volcanoes are not instrumented with in-situ sensors and even those that have sensor networks typicall have only a relatively small numbers of point sensors. Consequently, ideal volcanic study synergistically combines space and in-situ measurements

This paper describes an effort to integrate space-borne sensing from MODIS (Terra and Aqua), ALI (EO-1), Worldview-2, and in-situ sensing, in an automated scheme to improve global volcano monitoring. Specifically, we describe a "sensorweb" concept in which a number of volcano monitoring systems are linked together to more accurately monitor volcanic activity, and use this activity measurement to automatically task space assets to acquire further satellite imagery of ongoing volcanic activity. We discuss the space and ground sensors and systems and how they are linked together. We also describe results from operations of this system with a focus on the Earth Observing One mission as it has been executing a volcano monitoring campaign for over a decade.

Because the focus of this meeting is Artificial Intelligence (AI), we highlight the use of AI in the Volcano sensorweb, specifically in (1) intelligent event detection; (2) retasking EO-1 to observe detected volcano events; and (3) in automatic interpretation of volcanic events.

2 Volcano Event Detection using Space and Ground Triggers

Our volcano sensorweb uses a number of volcano monitoring systems to track volcanic activity worldwide (see Table 1 at the end of this paper). We incorporate numerous space-based and in-situ sensors to detect volcanic activity. However, in this section we focus on several detection agents that have a more Artificial Intelligence Component.

In 2008-2009 JPL, USGS/CVO and Washington State University collaborated to deploy a set of

wirelessly networked smart sensors [Huang et al. 2010]

Figure 1: Spider Sensor deployed to Mount Saint Helens in 2008 as part of Volcano Sensorweb

to Mount Saint Helens (See Figure 1). These sensors had sophisticated onboard smarts as well as network smarts and ground- to space and space to ground triggering and reconfiguration was demonstrated.

Specifically, on-node interpretation software used RSAM measures to detect seismic events and transmit data at a higher temporal resolution. Additionally, at the network level, based on these alerts and raw data, an extensible data analysis framework enables evidence and rule-based interpretation of events to adjust network quality of service QoS to allow this higher bandwidth of data (see Figure 2). This same interpretation software can issue alerts beyond the CVO to inform other entities as well as trigger space-based observations (e.g., EO-1).

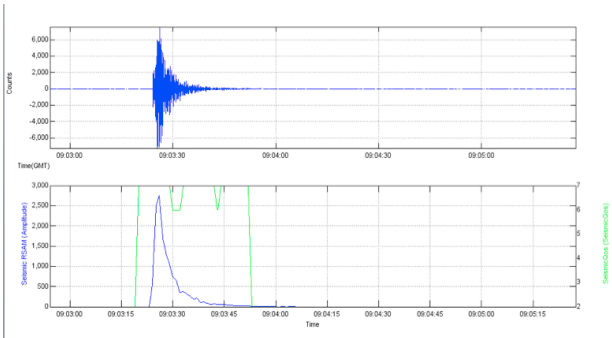

Figure 2: Example from OASIS Node 05 showing waveform, in-situ RSAM and in-situ event triggered QOS prioritization

The volcano sensorweb has been linked up with the monitoring network of in-situ sensors at Iceland run by the Iceland Met Office (www.vedur.is). The Iceland Met office has a sophisticated network of sensors to monitor volcanic activity in Iceland including seismographic, strain, GPS, and runoff sensors.

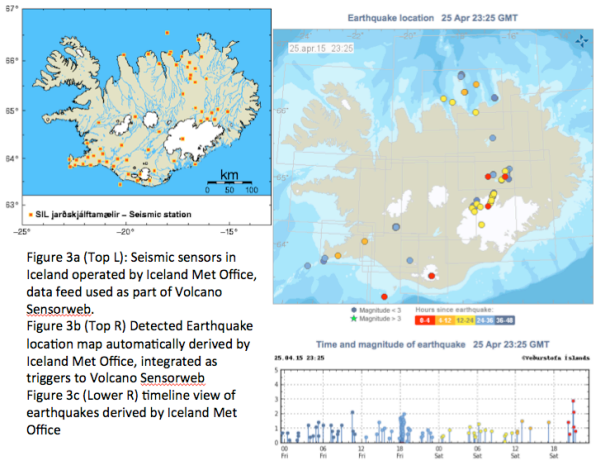

Figure 3a (Top L): Seismic sensors in Iceland operated by Iceland Met Office, data feed used as part of Volcano Sensorweb.
Figure 3b (Top R) Detected Earthquake location map automatically derived by Iceland Met Office, integrated as triggers to Volcano Sensorweb
Figure 3c (Lower R) timeline view of earthquakes derived by Iceland Met Office

The Volcano Sensorweb triggers space observations from seismic signatures (such as earthquake intensity, location, trending intensity, and shallowing depth). Specifically, since 2010, an operational software agent interprets the earthquake alerts from the Iceland Met Office. This software agent compiles evidence of a volcanic event where each earthquake event is assessed for its magnitude and proximity to known volcano locations. If the combined evidence, using an exponential fall-off model in time and distance, accumulates sufficient evidence to exceed an expert-derived threshold, an alert is issued and space-based observation requests are triggered.

We have also been investigating the potential to use stream flow rate sensors as indications of volcanic activity. Many Icelandic volcanoes are covered with glacier therefore increases in stream flow rates due to melting ice can be an early indicator of volcanic activity. While we have executed a manually triggered observation based on expert analysis of the situation, we have not yet developed an automatic sensorweb triggering mechanism of this type (see Figure 4 for examples of flow-rate data and observation).

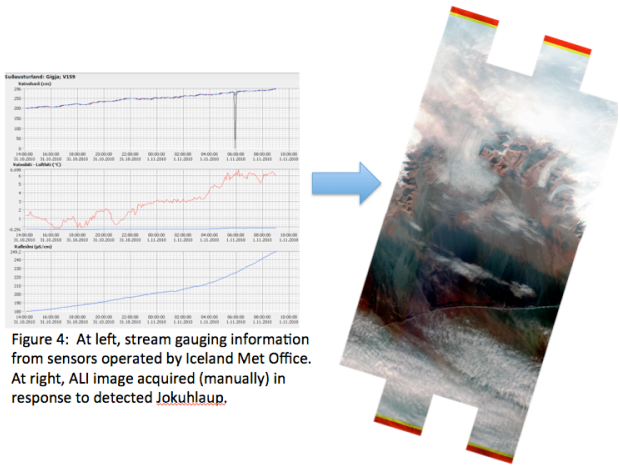

Figure 4: At left, stream gauging information from sensors operated by Iceland Met Office. At right, ALI image acquired (manually) in response to detected Jokuhlaup.

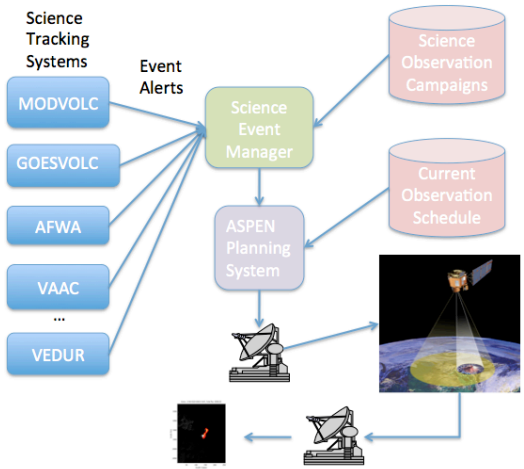

Figure 5: Automated flow from science event alert to observation request to acquired scene to delivered science products.

3 Automated Response Imagery Using Earth Observing One and the Autonomous Sciencecraft

The Earth Observing One (EO-1) spacecraft has automated tasking capability [Chien et al. 2005, Chien et al. 2010] that enables electronic submission of prioritized observation requests and automated retasking. The sensorweb uses the above alert systems to automatically task volcano observations based on scientist specified observation campaigns. The dataflow of this system is shown below in Figure 4. The sensorweb agents for the monitoring systems (e.g. MODVOLC, GOESVOLC, AFWA…) report the volcanic activity as "science alerts" which specify: location, event type, and other information such as confidence, size, severity, etc. The Science Event Manager processes the alerts and matches them up with scientist defined "observation campaigns" that describe situations in which science alerts or combinations of alerts result in observations requests or sets of requests. The EO-1 mission planning system (using the ASPEN system) then attempts to accommodate these observations requests while respecting spacecraft operations constraints and competing observation priorities.

ASPEN for EO-1 on the ground uses AI-based search combined with a timeline-based spacecraft modeling system [Chien et al. 2010] automate scheduling of EO-1 observations while respecting observation priorities and spacecraft operations constraints. The Autonomous Sciencecraft software (ASE) onboard also routinely analyzes the thermal data acquired to generate science summary products. ASE also uses the CASPER embedded scheduler version of the ASPEN software onboard to reschedule observations in light of events detected onboard [Chien et al. 2005].

4 Automated Analysis of Remote Sensed Volcano Imagery and Data Delivery

After the EO-1 data is acquired it is automatically processed for thermal signature extraction. Specifically, the Hyperion imagery is automatically processed onboard the spacecraft to derive surface temperature estimates using spectral slope estimation techniques [Davies et al. 2006] that can be downlinked very rapidly using engineering channel downlinks.

When the full imagery is downlinked automatic ground processing can derive still further information. On the ground a more complete analysis can provide estimates of volumetric lava effusion rates. [Davies et al. 2010] In this process, first, hot pixels are identified based on spectral signature. Next, each pixel is fitted to a blackbody radiation curve to derive a hot pixel area and temperature (e.g. an estimate that the pixel consists of a given area at ambient temperature and the remainder at a higher temperature). Finally, the data from each of these hot pixels are aggregated and matched to a volcanic model that then estimates the lava effusion rate based on the thermal signature, area, heat lossage, and lava composition.

4.1 Use of Machine Learning for automated volcanic ash detection in Worldview-2 data

Another usage of AI in the volcano sensorweb is the application of machine learning random decision forests to classify ash in Worldview-2 imagery [Mclaren et al. 2012].

4.1.1 WorldView-2 data, Radiometric and atmospheric correction

Our initial study used 10 WorldView-2 images acquired of the Eyjafjallajökull volcano in April and May of 2010. Of these 10 images, 2 contained no plume and 2 contained plume, but no plume shadow. As the presence of a plume shadow is needed to estimate plume height, our study therefore focused on the 6 remaining images.

We first converted these images to top-of-atmosphere reflectance [DigitalGlobe] before subsequent processing. However, this method still left considerable variance in brightness that hampered across-image analysis. We later switched to taking images not corrected to top-of-atmosphere reflectance and instead enhanced the contrast of each image using histogram equalization [Histogram]. We trained and ran our classifier on the histogram-equalized images. We oriented the resulting classification maps so that solar illumination came from the bottom of the image, using solar angles recorded in the observation metadata. Figure 6 shows a sample input image (at left) and a histogram equalized image (at right).

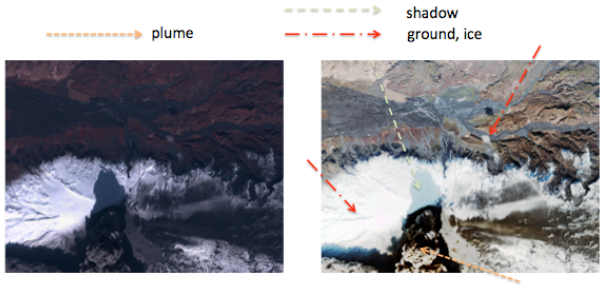

Figure 6: Worldview-2 Image (L) and Histogram-equalized WV-2 image (R) of Eyfjallajokull eruption, April 2010. Regions of plume, shadow, ground, and ice indicated.

4.1.2 Machine learning approach

We employ an image analysis technique method previously developed for in situ surface imagery. TextureCam [Thompson et al. 2012] is a framework and library of image processing and classification techniques intended for integration into a "smart" instrument. A machine learning strategy exploits manually labeled image regions to train a random forest classifier [Breiman 2001, Shotton et al. 2008]. We train this system to recognize the statistics of local image patches corresponding to: airborne ash plume, shadow, and other (including land, water, and ice). The learned classifier is intended to generalize to new scenes under different terrain and lighting conditions. It ascribes a probabilistic surface classification to each pixel that incorporates cues learned from multispectral intensity, local texture, local pixel statistics, and other image data.

In order to apply TextureCam to the WorldView-2 volcanic plume classification task we defined several input features. First, we specified all ratios of the 8 spectral bands available in WorldView-2 data, thus providing 28 features. The resultant decision trees derive the classification map shown in Figure 2, created by running the learned classifier on the image in Figure 6. Figure 7 (left) shows the probabilistic surface classification for the plume class, Figure 7 (middle) shows the probabilistic classification for the shadow class, and Figure 7 (right) shows the classification map for the other class.

Typical decision tree classifiers can provide a single label for each pixel based on the Maximum A Posteriori (MAP) classification - the most probable class of each datapoint. This label is based on image cues, but it is also influenced by the abundance of each class in the training images. For this reason it may not be the optimal solution for the specific accuracy requirements of the task. Consequently users often modify classification thresholds to favor one class or another. Our analysis uses classification thresholds that optimize the end goal of accurately estimating the anti-sunward edge of the ash plume and the extent of anti-sunward shadow adjacent to the ash. In order to further enhance accuracy we subsequently smooth and filter the classification map and apply segmentation techniques to sharpen the ash cloud boundary. Figure 8 shows the classification map for the image shown in Figure 6.

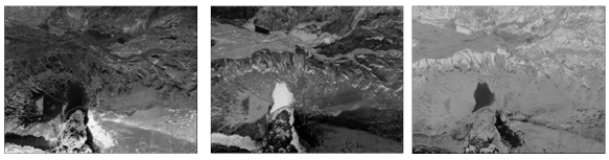

Figure 7: Probability maps derived from TextureCam (lighter = higher probability) for plume (left), shadow (center), other/land (right)

One of the key features of our interpretation method is that it should be scene, target, and illumination invariant. We trained the method on one image and applied it to a set of 5 different images (a total of 6 images in all). While all of the images were of the same target (the Eyjafjallajökull volcano) the images span two days and a range of viewing angles. Figure 4 shows the histogram equalized image (left) and classification map (right) on a separate Eyjafjallajökull observation acquired on a different day.

Our detection method is able to classify large areas of ash plume and shadow but experiences a number of difficulties:

1. *Dark portions of the ash plume are classified as shadows*. Indeed, due to the billowing nature of the ash plume, there are often large shadowed areas within the ash plume. Additionally, stair-step structure in the ash plume can also create large shadowed areas within the ash plume. We attempt to address this issue by smoothing the classification map to remove these smaller shadows out of the final ash plume classified region.
2. *Large areas of land are classified as ash plume*. Because our method relies on spectral features, land that may be covered with ash or spectrally

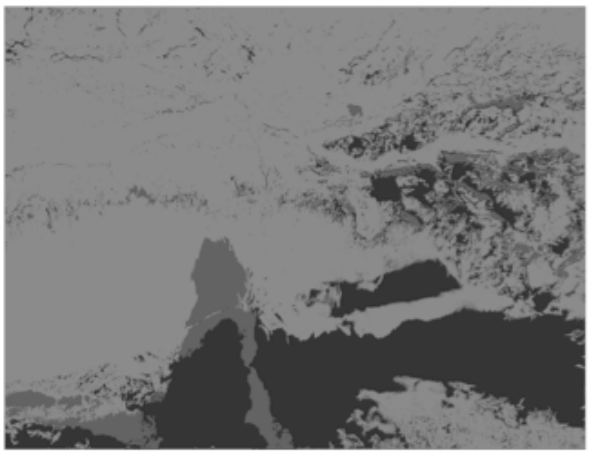

Figure 8: Integrated classification map where black = plume, grey = shadow, light = background/land.

similar materials may be misclassified as ash in a plume. We do not process these areas out but, because we are searching for shadow regions to the anti sunward side of ash plume regions, these types of misclassifications are unlikely to harm our calculations.

3. *Shadows may occur due to land features*. Because these areas are likely to be small and not have large ash regions to the sunward direction, they do not harm our calculations.
4. *Plume shadow is partially or fully out of frame*. Alternatively, the shadow may be in the image frame, but the plume is not. In general we discard plume and shadow estimates that run into the edge of the image.

Figure 9 shows a histogram-equalized image and class map indicating some of the classification difficulties. In particular, blue arrows highlight the difficulties in spectral based discrimination between ash plume and certain ground surfaces (in this case ash on the ground).

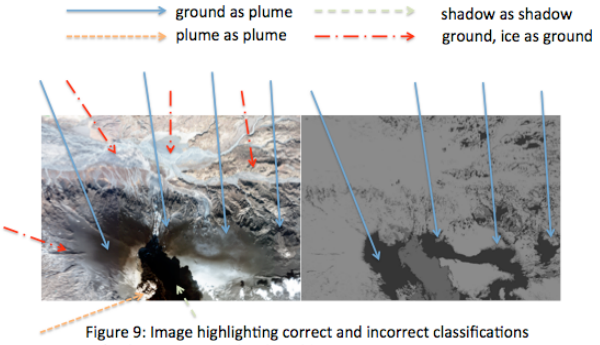

Figure 9: Image highlighting correct and incorrect classifications
Left – histogram equalized worldview-2 image
Right – classification map: black = plume, grey = shadow, light = land

Once the ash cloud and shadow has been identified, the image can be processed to estimate shadow length and therefore plume height above sea level [Prata & Grant 2001]. This algorithm works by finding line segments that run from sunward to anti-sunward direction that consist of a region of ash followed by a region of shadow. Each of these shadow measurements must then be corrected for:

1. relative position of the spacecraft;
2. relative position of the sun;
3. relative ground elevation of the shadow point;

to produce the estimate for the height of the plume edge above sea level. We utilize the ASTER GDEM2 digital elevation map (30 m horizontal spacing, 1 m vertical spacing) to correct for terrain effects.

One issue is that even assuming a perfect classification, our method produces an underestimate of plume because the plume possibly has a complex stair step structure rather than a single upward then windward structure. In order to address this difficulty we select the longest shadow rays that trace from large areas of plume, and compute plume heights corresponding to these rays. Figure 10 shows the geometric calculation being performed to extract the plume height.

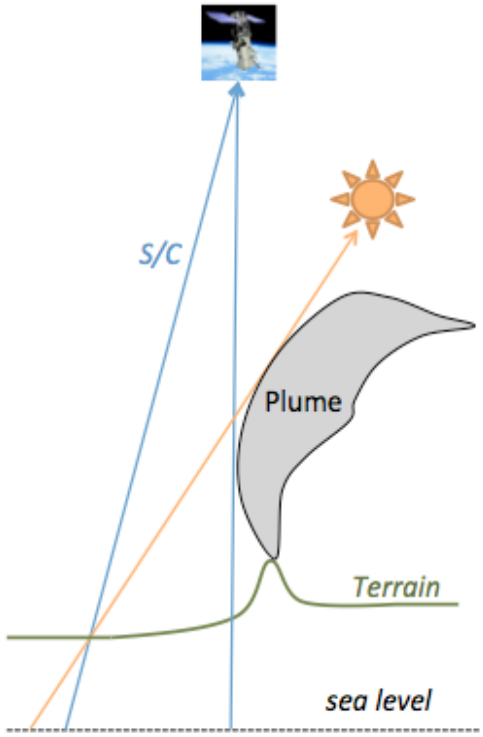

Figure 10: Visible shadow provides lower bound on plume height

We then compute the mean and standard deviation of the top quartile of plume height estimates, and discard all plume height estimates farther than two standard deviations from this mean. The remaining plumes constitute our final sample for analysis. For our best estimate, we report the mean of the plume heights in this sample. We also report the 20-80 percentile range of the remaining plume heights as an uncertainty estimate.

4.2 Plume Height Estimation for the 2010 Eyjafjallajökull eruption

We took the trained ash/shadow/background classifier from a single image from 17 April 2010 WorldView-2 overflight of the Eyjafjallajökull volcano and applied it that same image and to another 5 WorldView-2 images of the Eyjafjallajökull volcano. In all the images were acquired both 17 April and 11 May 2010 with a moderate range of lighting conditions with widely varying plumes. Table 2 at the end of the paper shows the estimated plume height ranges derived using the above shadow-based algorithms for each of the images. Table 2 also shows the independent visual and radar measurements [Arason et al. 2011] estimating the plume heights on the same days in question. The data shows reasonable agreement between the plume height estimated from WorldView-2 data and from other sources.

5 Impact of the Volcano Sensorweb – A Unique Dataset

The Volcano Sensorweb has been in operation tasking EO-1 for over 10 years and has acquired thousands of images. Figure 11 shows the distribution of Volcano Sensorweb alerts by type over the lifetime of the project (2004-present). Figure 12 shows a breakdown of volcanic images acquired by target type..

Figure 11: Volcano Science Alerts for 2004-2015- by Alert Source

Alert Source	Number of Alerts
VAAC	66565
MODVOLC	47963
GOES Hotspot	35492
AFWA	15031
MEVO	2232
HVO Tilt	386
HVO SO2	333
CVO Spider	79
Iceland VEDUR EQ	58
VSW Etna U. Firenze	54
VSW Ecuador	1

Figure 12: Volcano Images Acquired with EO-1 2004-2015 by Volcano Target

Number of Images	Volcanoes with this number of images acquired
500-1000	Erebus (970)
300-499	
100-299	Belinda, Heard, Rabaul, Shiveluch, Nyiragongo, Ambrym, Popocateptl, Erte Ale, Colima, Tungurahua, Piton de la Fournaise, Mt St Helens, Etna
50-99	Bagana, Anatahan, Karthala, Tolbachik, Yasur, Batur, Karymsky, Galunggung, Arenal, Home Reef, Dyngjujokull, Kliuchevskoi, Cleveland, Krakatau, Santa Maria, Sakura Jima, Shishaldin, Manam, Tinakalu,
1-49	50 volcanoes
1-9	90 Volcanoes

6 Conclusions

We have described a networking of science tracking, automated tasking, and data analysis systems into a sensorweb to enable global monitoring of volcanoes. This technique has enabled timely monitoring of unpredictable, varied, and short-lived volcanic activity.

Acknowledgements

The research was carried out at the Jet Propulsion Laboratory, California Institute of Technology, under a contract with the National Aeronautics and Space Administration.

References

Þ. Arason, G.N. Petersen and H. Björnsson, "Observations of the altitude of the volcanic plume during the eruption of Eyjafjallajökull, April-May 2010," Earth System Sciences Data, 3, 9-17 (2011).

L. Breiman, Machine learning 45(1):5 (2001).

S. Chien, R. Sherwood, D. Tran, B. Cichy, G. Rabideau, R. Castano, A. Davies, D. Mandl, S. Frye, B. Trout, S. Shulman, D. Boyer, "Using Autonomy Flight Software to Improve Science Return on Earth Observing One," Journal of Aerospace Computing, Information, and Communication, Apr. 2005, pp. 196–216.

S. Chien, B. Cichy, A. G. Davies, D. Tran, G. Rabideau, R. Castano, R. Sherwood, D. Mandl, S. Frye, S. Schulman, J. Jones and S. Grosvenor (2005a) An Autonomous Earth-Observing Sensorweb, IEEE Intelligent Systems, 20, no. 3, 16-24.

S. Chien, D. Tran, G. Rabideau, S. Schaffer, D. Mandl, S Frye, "Timeline-based Space Operations Scheduling with External Constraints, " International Conference on Automated Planning and Scheduling, Toronto, Canada, May 2010.

A.G. Davies et al., "Monitoring Active Volcanism with the Autonomous Sciencecraft Experiment (ASE) on EO-1," Remote Sensing of the Environment, vol. 101, no. 4, 2006, pp. 427–446.

A. G. Davies, S. Chien, R. Wright, A. Miklius, P. R. Kyle, M. Welsh, J. B. Johnson, D. Tran, S. R. Schaffer, and R. Sherwood, "Sensor web enables rapid response to volcanic activity," Eos, vol. 87, no. 1, pp. 1–5, 2006.

A. Davies, S. Chien, D. Tran, J. Doubleday, "Onboard Processing of Multispectral and Hyperspectral data of Volcanic Activity for Future Earth Orbiting Missions," International Geoscience and Remote Sensing Symposium, Honolulu, HI, July 2010.

Davies, A. G., Chien, S., Tran, D. and Doubleday, J. (2015) The NASA Volcano Sensor Web, Advanced Autonomy, and the Remote Sensing of Volcanic Eruptions, Chapter in the Geological Society of London-IAVCEI book "Detecting, Modeling and Responding to Effusive Eruptions", eds. A. J. L. Harris, T. De Groove, P. Labazuy and S. Carn, in press.

DigitalGlobe, ***worldview2****.digitalglobe.com, (2012).*

DigitalGlobe, "Radiometric Use of WorldView-2 Imagery." Technical Note. Accessed March 2, 2012. http://www.digitalglobe.com/downloads/Radiometric_Use_of_WorldView-2_Imagery.pdf, (2012).

A. J. Harris, Flynn, L. P., Dean, K., Wooster, E. M., Okubo, C., Mouginis-Mark, P., et al. (2000). Real-time satellite monitoring of volcanic hot spots. Geophysical Monograph, vol. 116 (pp. 139– 159) pub. AGU.

Wikipedia, “Wikipedia: Histogram Equalization,” http://en.wikipedia.org/wiki/Histogram_equalization, retrieved 13 March (2012).

R. Huang, M. Xu, N. Peterson, W. Song, B. Shirazi, R. LaHusen, J. Pallister, D. Dzurisin, S. Moran, M. Lisowski, S. Kedar, S. Chien, F. Webb, A. Kiely, J. Doubleday, A. Davies, D. Pieri, “Optimized Autonomous Space In-situ Sensor-Web for Volcano Monitoring,” IEEE Journal of Selected Topics in Applied Earth Observations and Remote Sensing, 2010.

EOS - Earth Observatory Image of the day, http://earthobservatory.nasa.gov/NaturalHazards/view.php?id=46693

D. Mclaren, D. R. Thompson, A. G. Davies, M. Gudmundsson, S. Chien, “Automatic estimation of volcanic ash plume height using Worldview-2 imagery,” SPIE Defense, Security, and Sensing. Algorithms and Technologies for Multispectral, Hyperspectral, and Ultraspectral Imagery XVIII. Baltimore, MD. April 2012

A. J. Prata and I. F. Grant, “Determination of mass loadings and plume heights of vol- canic ash clouds from satellite data,” *CSIRO Atmospheric Research and Technology Papers* **48**, 39, Commonwealth Science and Industry Research Organization, Melbourne, Victoria, Australia (2001).

Schölkopf, B., & Smola, A. J. (2002). Learning with kernels. Cambridge, MA: MIT Press.

J. Shotton, M. Johnson, R. Cipolla, “Semantic texton forests for image categorization and segmentation,” IEEE Conf on Computer Vision and Pattern Recognition 1–8 (2008).

D. R. Thompson, A. Allwood, D. Bekker, N. A. Cabrol, T. Estlin, T. Fuchs, K. L. Wagstaff, "TextureCam: Autonomous image analysis for astrobiology survey," Lunar and Planetary Sciences Conference, Houston, TX, (2012).

Wright, R., Flynn, L. P., Garbeil, H., Harris, A., & Pilger, E. (2002). Automated volcanic eruption detection using MODIS. Remote Sensing of Environment, 82, 135– 155.

Wright, R., Flynn, L. P., Garbeil, H., Harris, A. J. L., & Pilger, E. (2004). MODVOLC: Near-real-time thermal monitoring of global volcanism. Journal of Volcanology and Geothermal Research, 135, 29–49.

Data source	Asset name/location	Data source	VSW Trigger	Coverage	VSW operational history	References	Notes
1. Spacecraft data processing application	*EO-1* – ASE (Autonomous Sciencecraft)	Hyperion spectrometer	Detection of hot pixels	Global	2004-	(Chien et al., 2005b; Davies et al., 2006a)	Autonomous science-driven spacecraft operations
1. Spacecraft data processing application	MODVOLC (University of Hawai'i)	Earth-orbiting MODIS instruments	Detection of hot pixels	Global	On-line since 2005	(Wright et al., 2002; Wright et al., 2004)	MODIS is on the NASA *Terra* and *Aqua* spacecraft
1. Spacecraft data processing application	GoesVOLC (University of Hawai'i)	Platforms in geostationary orbit	Detection of hot pixels	Primarily Hawai'i; Pacific rim volcanoes	Online 2005-2006	(Davies et al., 2006b; Harris et al., 1997; Harris and Thornber, 1999)	*GOES* spacecraft in geostationary orbit, observing Pacific and Pacific rim
2. In situ instrumentation	Mount Erebus Volcano Observatory	Acoustic sensors	Strombolian event detection	Mount Erebus, Antarctica	2004-2007	(Aster et al., 2004; Davies et al., 2006a)	Erebus Volcano Observatory is operated by New Mexico Tech, Socorro, NM
2. In situ instrumentation	USGS Hawaiian Volcano Observatory (Hawai'i)	VALVE – tiltmeter network	Tilt behavior indicative of impending eruption	Kilauea, HI	2005-2006, 2014-	(Cervelli and Miklius, 2003)	VALVE incorporates tilt, seismic, gas data and automatically issues alerts. In 2014: tiltmeter network.
2. In situ instrumentation	USGS HVO / NPS-HVNP (Hawai'i)	Volcano Monitors (VM)	Anomalous SO_2 detection	Kilauea, HI	2006-2008	(Boudreau et al., 2007; Davies et al., 2008c)	Demonstrated *EO-1*- VM two-way triggering via VSW
2. In situ instrumentation	USGS Cascades Volcano Observatory (Vancouver, WA)	Volcano-monitoring deployable stations "Spiders" (seismic, acoustic, gps)	Seismic alert	Mt. St. Helens, WA	2010-	(LaHusen et al., 2010); (Chien et al., 2010)	Fastest trigger-observation response obtained so far: 2 hours (3 July 2005) from CVO seismic event detection.
2. In situ instrumentation	Iceland Meteorological Office	Seismic, tilt, melt water flow metering	Seismic alert	Iceland volcanoes	2010-	Davies et al., 2013	Grimsvötn 2011 eruption (see Appendix 2 in Davies et al., 2013).
2. In situ instrumentation	University of Firenze, Italy	Acoustic sensors	Explosions	Etna	2012-2014	Marchetti et al., 2011	Successful triggers of *EO-1* observations in 2013 and 2014
2. In situ instrumentation	Institute for Geophysics for Ecuador (IGEPN)	Seismic	Seismic alert ("State of the Volcano")	Tungurahua, Reventador	2013		Specifically requests ALI daytime data to determine location and plume extent
3. Ash advisory	Volcanic Ash Advisory Center (VAAC) alerts (7 centers)	Multiple (e.g., pilot reports)	Plume detection	Global	2005-	(Davies et al., 2006b)	Many alerts world-wide, inc. Talang, 2005; Nyamulagira, 2006; Nishino-Shima, 2013
3. Ash advisory	US Air Force Weather Agency (AFWA) alert	Multiple (e.g., pilot reports)	Plume detection	Global	2005-		Multiple detections and triggers
4. Other reports of eruptions	Multiple notification sources	Alert of impending or ongoing activity from news media, colleagues	Manual	Global	2004-		Numerous events around the world, inc. Afar eruptions (Ethiopia/Eritrea), 2006-2011; Puyehue Cordon Caulle (Chile), 2011-2012

Table 1: Volcano Sensorweb Linkages. Reproduced with permission from [Davies et al., in press].

Image	Plume height estimate (in km above sea level)				
	WorldView-2 Shadow-based Estimates			Estimates from [Arason et al. 2011]	
	# of samples	Best estimate (mean) (in km)	20^{th} - 80^{th} %-ile Range (in km)	Visual Estimate	Radar Estimate
17 April 2010	290	2.66	2.52-2.97	2.3-5.5km (Figure 9)	4.8-8.5km (Figure 9)
17 April 2010	199	3.57	3.51-3.64		
17 April 2010	585	3.06	2.94-3.15		
17 April 2010	8	4.35	4.35-4.36		
11 May 2010	12	3.02	3.02-3.03	3.8-4.4 km, mean=4.3km (Figure 10)	3.6-4.9 km, mean = 4.3km (Figure 10)
11 May 2010	154	4.58	4.47-4.67		

Table 2: Comparison of plume height estimates from WorldView-2 shadow based derivation to visual and radar measurements from [Arason et al. 2011] for WorldView-2 scenes from 17 April 2010 and 11 May 2010.